Eur. Phys. J. Plus (2015) **130**: 160
DOI 10.1140/epjp/i2015-15160-y

THE EUROPEAN PHYSICAL JOURNAL PLUS

Review

The crystallography stations at the Alba synchrotron*

François Fauth, Roeland Boer, Fernando Gil-Ortiz, Catalin Popescu, Oriol Vallcorba, Inma Peral, Daniel Fullà, Jordi Benach[a], and Jordi Juanhuix[b]

Alba Synchrotron, BP 1413, km 3.3, Cerdanyola del Vallès, Spain

Received: 11 June 2015
Published online: 10 August 2015 – © Società Italiana di Fisica / Springer-Verlag 2015

Abstract. Alba is a 3rd-generation 3 GeV synchrotron facility with an emittance of 4.6 nm · rad which has been operational since 2011 and has recently started top-up operation. Photons in a broad energy range of 0.08–80 keV are served to seven beamlines dedicated to a large variety of scientific fields. The portfolio includes two beamlines, XALOC and MSPD, fully dedicated to X-ray crystallography. BL13-XALOC is currently the only macromolecular crystallography beamline. The end-station includes a high-accuracy single-axis diffractometer with a removable minikappa stage, a sample-mounting robot and a large-area, photon-counting detector. The beamline optics, fed by an in-vacuum undulator, deliver a tunable photon beam between 5.5 and 22 keV. The beam size at the sample position can be adjusted by defocusing the mirrors in a range of 50–300 μm in the horizontal direction and 5.5–300 μm in the vertical direction. Beamline BL04-MSPD, which is fed by a superconducting wiggler, has two in-line end-stations. The first station is devoted to high-pressure/microdiffraction. It offers a 15×15 μm beam in the range 20–50 keV, particularly suited for powder diffraction studies requiring a very small beam, *e.g.* mapping of cultural heritage samples and high-pressures studies. The second station is dedicated to high-resolution/high-throughput powder diffraction. It covers the 8–50 keV range and includes a heavy-duty 3-circle diffractometer equipped with a 13-channel multianalyzer detector with high-angular resolution ($\Delta 2\theta = 0.004^\circ$ FWHM) and a high-throughput, position-sensitive detector spanning 40° in 2θ range allowing millisecond data acquisitions.

1 Introduction

In the last decade, a number of national synchrotron facilities have come into operation to provide a readily accessible X-ray photon source to the respective regional scientific communities, while fully opening the facility to the worldwide community and to industry. This is indeed the case of the Alba synchrotron light facility, which has been built near Barcelona (Spain). Alba has been constructed and is being operated by CELLS (the Consortium for Construction, Equipment and Exploitation of the Synchrotron Light Laboratory), a consortium that receives its funding in equal shares from the Spanish government (via the Science Ministry) and the Catalan government (via the Department of Research and Universities). The project was approved in 2003, construction started in 2006 and the first synchrotron light was produced in 2011. The commissioning of the beamlines started fall 2011 and took between 6 and 18 months. The first external users were hosted by mid-2012.

Alba storage ring has a circumference of 268 m, and accommodates a stable electron beam at an energy of 3 GeV and a measured emittance of 4.6 nm · rad [1]. The storage ring initially operated at a current of 120 mA in decay uniform-filling mode but, by mid-2014, operation was switched to top-up mode. Over the next two years, the current is scheduled to increase gradually to a nominal value of 250 mA. The storage ring presently feeds X-ray photons to seven operating beamlines, dedicated to diverse scientific fields, which require photons with energy between 80 eV and 80 keV (fig. 1). Three beamlines are devoted to techniques using photons in the soft X-ray range (resonant absorption scattering, photoemission spectroscopy and microscopy, X-ray microscopy), whereas four are using photons in the

* Contribution to the Focus Point on "Status of third-generation synchrotron crystallography beamlines: An overview" edited by Gaston Garcia.

[a] *Present address*: LRL-CAT, Eli Lilly and Company, Advanced Photon Source, Argonne National Laboratory, Building 438A, 9700 S. Cass Ave., Lemont, IL 60439 USA.

[b] e-mail: juanhuix@cells.es

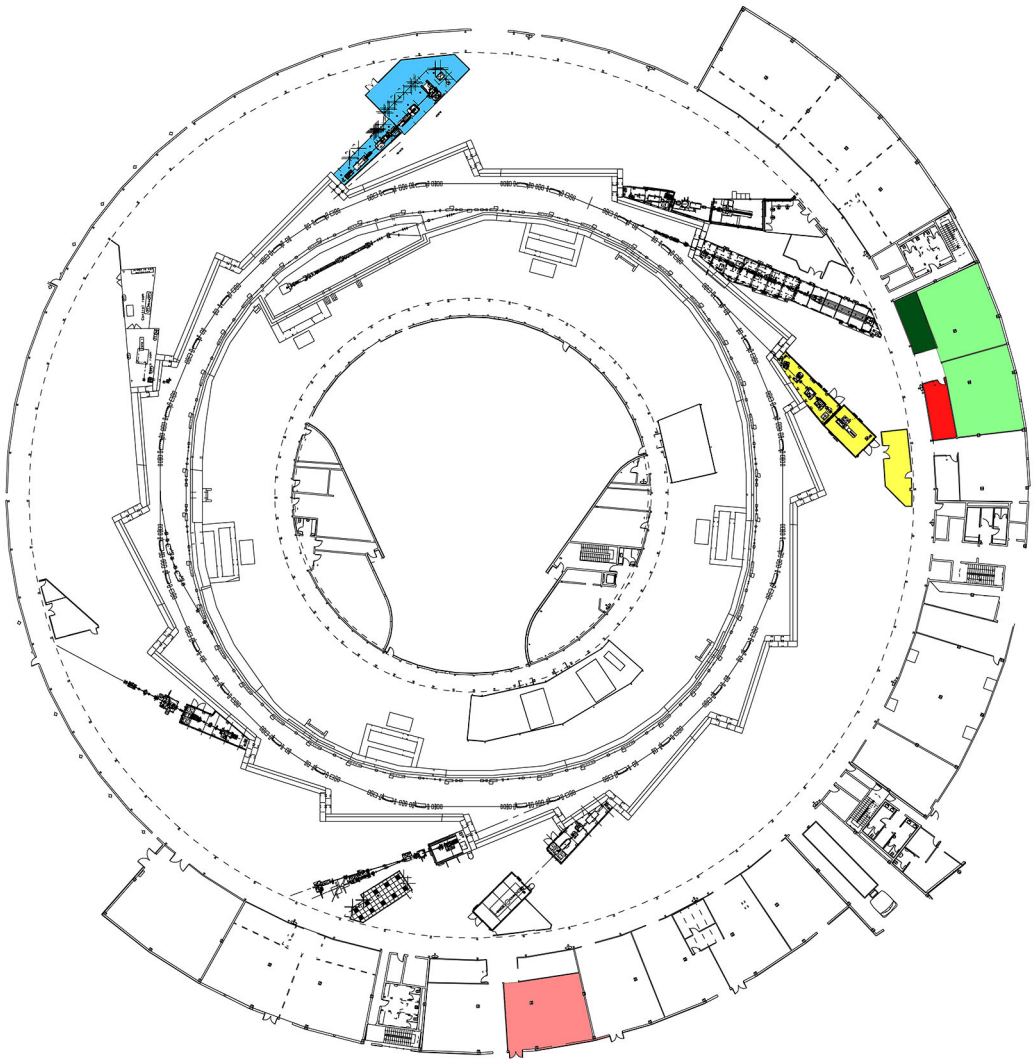

Fig. 1. Layout of the Alba experimental hall with the seven beamlines already built in the first phase. BL13-XALOC and BL04-MSPD beamlines are marked in yellow and blue, respectively. The biological laboratories are marked in green (cold room in dark green), and chemistry laboratory is marked in pink (high-pressure lab is marked in red).

hard X-ray range (non-crystalline diffraction, absorption and emission spectroscopy, macromolecular crystallography, powder diffraction). Two additional beamlines are funded and currently under design and construction (angular resolved soft X-ray spectroscopy and infrared spectroscopy) and will be operational by 2017. Finally, the selection of the next-to-be-built beamlines will be announced during 2015.

The beamlines have nearby three specialized laboratories dedicated to biological, chemical and materials science experiments, respectively, which are fully equipped to prepare samples and provide support to the experiments (fig. 2). The laboratories have a total surface area of approximately 400 m^2. The biological laboratory includes a 10 m^2 cold room at 4 °C and a small lab to perform activities requiring biosafety level 2. The chemistry lab is equipped with an Ar-filled glovebox, well suited for loading cells used in electrochemical experiments, and a tubular furnace (max 1200 °C) allowing sample manipulation under neutral gas atmosphere. There is also a laboratory dedicated to high-pressure studies equipped with two microscopes, a gasket drilling machine and a ruby fluorescence pressure calibration setup allows loading and testing diamond anvil cells (DAC) prior to measurements.

Beam time at Alba beamlines is allocated to academic users worldwide through peer-review proposals submitted through the Alba web user portal (`http://useroffice.cells.es`). There are two calls for proposals per year for all beamlines, except for the BL13-XALOC beamline, which has one annual call. Beam time is also sold to industrial users via the industrial liaison office. Two out of the seven operating beamlines are dedicated to X-ray crystallography techniques: macromolecular crystallography (BL13-XALOC beamline) and material science and powder diffraction (BL04-MSPD beamline).

Fig. 2. General views of the perimetral laboratories servicing the beamlines users: (a) Biological laboratory; (b) chemistry laboratory. Other dedicated laboratories available are: high pressure, cold room, biosafety level 2.

2 The BL13-XALOC beamline

BL13-XALOC is currently the only macromolecular crystallography (MX) beamline at Alba. XALOC has been designed with the aim to provide maximum coverage for the broad diversity of MX projects, using a generalist approach to cope with standard, automatable X-ray diffraction experiments of medium-sized crystals, as well as with more complex non-standard experiments that include a variety of crystal sizes and unit cell length dimensions, crystals with high mosaic spread, or poorly diffracting crystals. This generalist approach contrasts with other synchrotron facilities hosting several beamlines, each of which tends to focus on specific techniques or specific characteristics of the crystals. The XALOC beamline source, optics and end-station provide a stable beam and allow a flexible operation in terms of photon energy and beam size at sample, which can be changed by focusing or defocusing the beam at the sample position through appropriate bending of the mirrors.

2.1 The beamline optics

The photon source of the XALOC beamline is a 2 m long pure-permanent magnet in-vacuum undulator (IVU21) manufactured by Bruker Advanced Supercon (formerly ACCEL) (Bergisch Gladbach, Germany), placed in a medium straight section of the Alba storage ring [2]. The undulator has a minimum gap of 5.7 mm and a magnetic period of 21.6 mm. The design optimizes the undulator at the most used energy in MX experiments, *i.e.* the Se K-edge (12.658 keV), while providing a high flux in the 5–22 keV energy range, thus covering the majority of the absorption edges used in MX to solve the crystal structures through anomalous phasing. The resulting photon source is $310\times18\,\mu$m in size, whereas the source divergence is $112\times25\,\mu$rad (H×V, FWHM). The source size and divergence in both directions are limited by the electron beam emittance, while the vertical divergence is also limited by the energy spread of the electron beam. The first element of the beamline optics is an 8 mm diameter aperture, 400 μm thick diamond window, which separates the front-end and the beamline vacuum sectors and absorbs most of the beam power below 5 keV.

The basic elements of the beamline optics are a channel-cut monochromator and a pair of focusing mirrors in a Kirkpatrick-Baez (KB) configuration (fig. 3). The monochromator is a cryogenically cooled, channel-cut double crystal monochromator that uses the reflection (111) from Si and was manufactured by Cinel s.r.l. (Vigonza, Italy). The stability of the monochromator was increased by modifying the cryocooling circuit to allow the working point of the liquid N_2 flow to be closer to the laminar regime using finite element analysis. The vibrational tests showed that the first resonance of the monochromator mechanics is well above 150 Hz [3].

The focusing system of the beamline consists of a vertical focusing mirror (VFM) and a horizontal focusing mirror (HFM) placed orthogonally in a Kirkpatrick-Baez (KB) configuration [4] in two independent positioning supports manufactured by IRELEC (Saint-Martin-d'Hères, France). The optical surfaces, manufactured by InSync Optics (Albuquerque, NM, USA), are made of silicon and have three stripes (bare Si, Rh coating and Ir coating) to provide a good suppression of the third harmonic from the monochromator over the full energy range. The optical surfaces are planar, with an optical length of 300 mm and 600 mm for the VFM and HFM, respectively. The mirrors are elliptically bent in the meridional direction by two independent stepper motors. The mirrors are designed to allow working under different focusing conditions to allow for a variable size of the beam at the sample position without losing flux by cutting the beam using slits. This imposes strong requirements on the slope errors of the mirrors to avoid striations

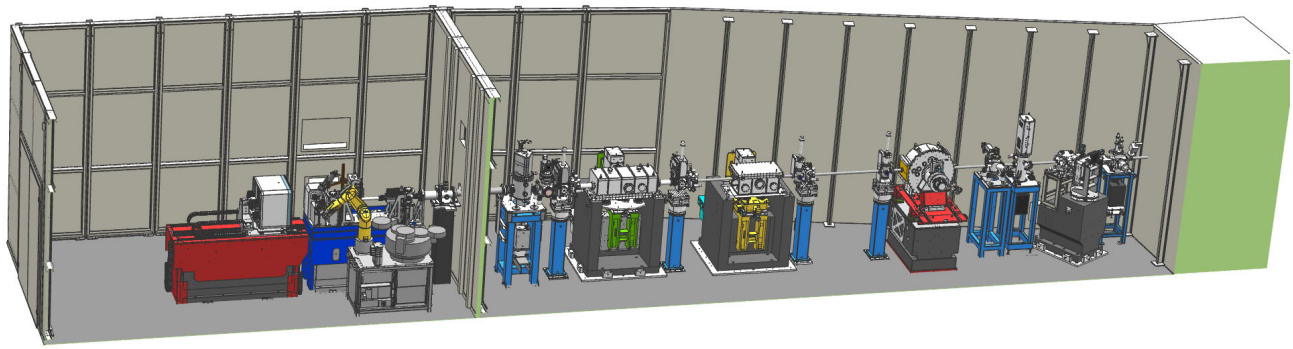

Fig. 3. Layout of the BL13-XALOC beamline.

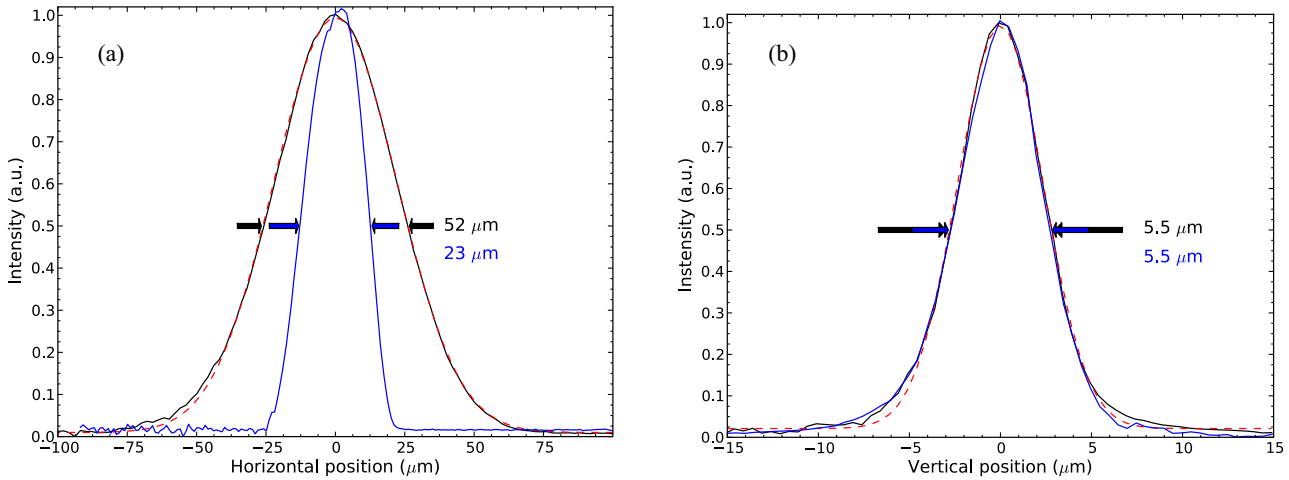

Fig. 4. Beam size at sample position in the horizontal and vertical dimensions, measured by scanning a knife-edge tungsten blade through the beam profile in the corresponding direction. Black curves correspond to full beam profiles (Gaussian fit in dashed red line). Blue lines correspond to the beam passing through a 30 μm diameter aperture placed 30 mm before the sample.

in the beam that typically appear due to surface errors, especially in the vertical profile [5]. To minimize these striations, we have developed a new method that corrects large-sized mirrors by using mechanical spring actuators [6]. The method is based on the classic elastic beam theory and a high-accuracy profile metrology provided by the Alba-NOM instrument at Alba [7]. The optimization led to a reduction of the RMS slope errors from 180 nrad to 55 nrad for the VFM, and from 210 nrad to 83 mrad for the HFM. It is worth noting that the optical surface of the VFM is long enough to cope with the whole vertical profile of the beam as well as with the differential vertical excursion of the beam related with the selection of a different energy using the channel-cut monochromator. Consequently, the mirrors do not need adjustment when changing the energy, and the positional change of the beam at the sample position is corrected using only the diffractometer positioning table.

2.2 The experimental station

The beamline optics delivers an X-ray beam to the experimental station that is easily tunable between 5.5 and 22 keV and has a Gaussian spot size at the sample position that can be adjusted in a range of $52 \times 5.5\,\mu m^2$ to $300 \times 300\,\mu m^2$ (beam FWHM, H $\times$ V). The beam size can be further reduced by using a 30 μm diameter aperture (fig. 4). The main characteristics of the beam at the sample position are listed in table 1. The end-station (fig. 5) is based on two high-precision positioning tables that independently adjust the diffractometer and the detector positions. The tables are the key to accurately and reliably align the sample with the X-ray beam after changing the photon energy or the optical configuration. Their design is based on mechanical flexures to increase the stiffness and the frequency of the resonant vibrational modes, which have been measured to be above 40 Hz. The beam-conditioning and diagnostic elements consist of a set of 12 attenuators, a fast shutter, a set of slits, and two CVD diamond 4-quadrant beam position monitors.

The sample is mounted in a single-axis (ω) MD2M diffractometer (Maatel-Bruker, Moirans, France), which shows a measured repeatability of 0.048 mdeg, a sphere of confusion of around 1 μm, and a RMS following error of 0.2 mdeg. This

Table 1. Beam characteristics of the BL13-XALOC beamline at the sample position.

Energy range	5.5–22 keV (2.25–0.55 A)
Energy dispersion ($\Delta E/E$)	2.0×10^{-4}
	(as measured through a rocking curve scan)
Minimum beam size at sample (focused)	$52 \times 5.5\,\mu m^2$ (H × V, FWHM)
	(as measured using a knife-edge scan and a PIN diode)
Beam divergence at sample	$600 \times 90\,\mu rad$ (H × V, FWHM)
	(as calculated from beam sizes at source and sample position)
Flux at 12.658 keV at sample position	$\sim 2 \times 10^{12}$ photons s^{-1} at 250 mA
	(as measured using an IRD AXUV36 PIN diode)

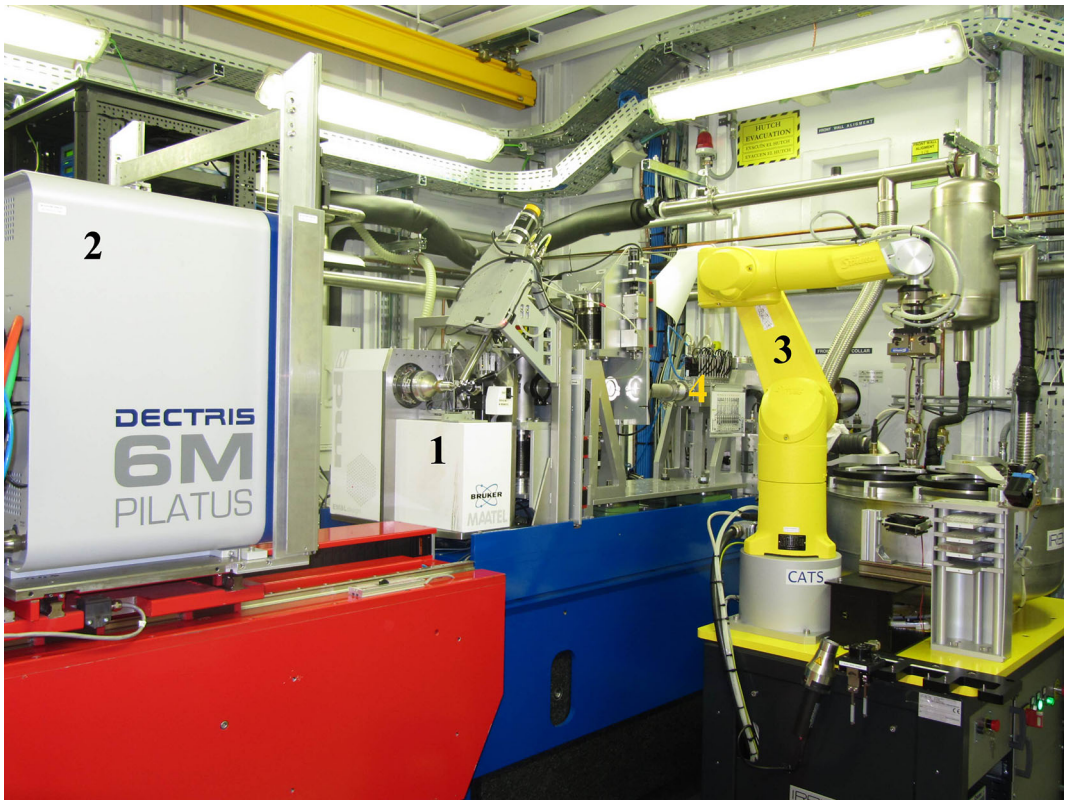

Fig. 5. End-station of the BL13-XALOC beamline dedicated to macromolecular crystallography. The main elements are the diffractometer (1), the pixel-array detector (2), the automatic sample changer (3), and the beam conditioning elements (4).

performance allows high-accuracy diffraction experiments using the oscillation method. If needed by the user, a mini-kappa mount (MK3) that adds two extra degrees of rotation (κ and φ), can be easily mounted on the diffractometer. The MK3 is useful to collect complete data at high resolution and to optimize anomalous data collections, although it increases the sphere of confusion to $< 5\,\mu m$. The MD2M diffractometer also includes an on-axis sample viewing system, and an exchangeable beam-stop (300 to 700 μm diameter) coupled to a capillary with a cleaning aperture (200 μm or 350 μm diameter) to remove stray light. The sample can be kept at cryogenic conditions with an Oxford Cryostream 700 (Oxford cryosystems, Oxford, UK).

A cryogenic automated transfer system robot, or CATS (IRELEC, Saint-Martin-d'Hères, France) [8], is handling cryogenic samples mounted in standard SPINE pins at the beamline. The cryosamples are stored in a LN_2 Dewar that can store 90 SPINE vials/caps, which can be identified by reading the standard dot matrix barcode printed on the caps. CATS operates reliably with a low failure rate of $< 1\%$ over 3000 mounted samples, provided that the relative humidity in the hutch is less than 30%. The samples can be mounted on different positions of the diffractometer, coping with the adjustment in position due to the photon energy or the optical configuration.

The main data collection detector is a photon-counting Pilatus 6M (DECTRIS Ltd, Baden, Switzerland) [9] that can be positioned at 123.5–1356 mm from the sample and is operated in shutterless mode. The Pilatus 6M detector

offers a large sensitive area (431 mm × 448 mm), a fast framing rate (12.5 Hz), a large dynamic range (20 bits), a negligible dark-current noise and a point spread function of 1 pixel. The data acquisition can be synchronized with the oscillation axis either for each image or at the beginning of the data collection. The beamline is also equipped with a Si-drift fluorescence detector X-Flash 410 (Bruker AXS Microanalysis GmbH, Berlin, Germany) to obtain fast and accurate XANES spectra and to select the optimal X-ray energy for SAD/MAD experiments.

Finally, the beamline control system is based on Sardana, a new supervision, control and data acquisition package inspired in the TANGO Collaboration [10]. Sardana is implemented in all the other beamlines at Alba as well as in the Alba accelerator complex. Currently, MX experiments at XALOC are performed through independent widgets which control the beamline instrumentation (sample-viewing system, automatic sample changer, fluorescence scans, etc.). Complex data acquisitions such as batch, inverse-beam data collections and raster scans to locate the crystal inside loops are being implemented. Remote data collection is expected to be supported in the forthcoming year.

3 The BL04-MSPD beamline

The Material Science Powder Diffraction beamline (BL04-MSPD) is the Alba facility dedicated to crystallography of material in powder form. The beamline consists of two experimental stations positioned in series; the first one specializes in high pressure/micro diffraction (HP/MD), the second in high-angular resolution/high-throughput standard powder diffraction. Owing to its extended energy range, 8–50 keV, the BL04-MSPD covers the requirements of most powder diffraction techniques: *ab initio* structure determination/crystal structure refinement of either organic or inorganic materials, total scattering/pair distribution function methods, strain/stress scanning of engineering-based compounds and *in operando* powder diffraction techniques (electrochemistry, pump probe experiments).

3.1 The beamline optics

The beamline conceptual design of its components have already been subject of previous reports [11] and [12], here we summarize the overall optical design outline. In order to reach the upper side of the 8–50 keV energy range without significant intensity loss, a superconducting wiggler (Budker Institute, Novosibirsk) was chosen as the insertion device (ID). It has a fixed magnetic gap distance (12.6 mm) and 117 full-field pole pairs of 30.16 mm period. A peak on-axis magnetic field of 2.16 T can be reached by tuning an electric current through NbTi coils that are assembled symmetrically above and below the vacuum chamber (8 mm height) and plunged into a liquid helium bath. Under these conditions, the deflection parameter (K) and critical energy (E_c) are 6.08 and 12.9 keV, respectively. At the typical energy of 30 keV and assuming a ring current of 200 mA, calculations using the SPECTRA 7.1.1 software [13] yield an effective X-ray source size, divergence and flux of $620 \times 85\,\mu m^2$, $1 \times 0.16\,mrad^2$ and 4.58×10^{13} ph/s/0.1%bw within a 1.5 × 1.5 mm front-end aperture, respectively. The latter aperture corresponds to that used for standard operation and of course reduces the total flux by a factor ~ 20 compared to full acceptance opening. The flux in the soft energy range (< 10 keV) is further damped by a factor ~ 1.5–2 owing to the insertion of two CVD windows as interfaces between the machine and the BL04 optics and a Be window separating the ultra-high vacuum of the beamline and the air in the experimental hutch. The flux in the full operating energy range varies smoothly within one order of magnitude.

A fixed exit (20 mm offset) double crystal monochromator (DCM) is located 25 m downstream of the photon source and was delivered by Bruker. Based on the double Bragg reflection of silicon (111) planes, it allows to select X-ray energies down to $\Delta E/E \sim 10^{-4}$ resolution. In order to reduce the heat load impact on energy resolution, both crystals are cryogenically cooled. An additional water circulation system allows to thermalize the crystal mounting mechanics, hence reducing long time mechanical drift due to white beam intensity variation (*e.g.*, after refill or machine shutdown). The monochromatic beam energy is selected by rotating the double-crystal assembly. The 2nd crystal has an additional rotation freedom driven either by a stepper motor or by a piezo actuator, the latter offering a finer tuning and allowing a feedback control in order to keep a constant ratio of outgoing *versus* incoming beam. This option is particularly useful when the storage ring is not operating in top up mode. It has to be noted that the maximal operating energy of the beamline, 50 keV, is limited by the length of the 2nd crystal.

A collimating mirror is inserted between the source (at 21 m) and the monochromator, which reduces the heat load downstream of the line, reduces the vertical divergence and eliminates high-energy harmonics. The mirror is essentially a water cooled 1.2 m long silicon block. A single motor actuation mechanism allows curving cylindrically the mirror down to a 5 km radius. Since the mirror is in a fixed position at an incident angle of 2 mrad relative to the incoming beam, the vertical collimation and focalization at the powder station (35 m from the source) are reached using a 21 km and 8.4 km bending radius, respectively. The mirror has three material surfaces since, in addition to the raw Si based surface, two 19 mm wide stripes are layered coated (~ 600 Å thickness) with Rh and Pt. Each of the three layered stripes surface offers a characteristic reflectivity curve with energy cut-offs of approx. 15 keV, 33 keV and 41 keV for Si, Rh and Pt, respectively. This energy cut off distribution is used to select the optimum surface layer in order to

eliminate the 3rd harmonics of the energy spectrum which can propagate downstream of the monochromator. In order to operate in the 40–50 keV range, the mirror is moved out of the white beam. In this operation mode, the heat load on the monochromator is lowered by reducing the beam size, either by using the slit system at the front-end and/or by using an equivalent slit system positioned between the mirror and the monochromator. Note that the option to operate with or without mirror implies that all mirror downstream components have to be vertically adjustable (up to 56 mm offset at the PD station). In the collimating mode, the specified 1.5 μrad slope error of the mirror surface was expected to ensure, under heat load, a residual 10 μrad vertical divergence of the synchrotron beam in the whole energy range. It is this reduced divergence, together with the low-energy band pass of the monochromator, which contributes to obtain the optimum high angular resolution in powder diffraction techniques [14]. However so-called striation effects [15] lead to a structured —non-Gaussian— vertical beam profile that can affect the measured peak profile, which makes modeling of the collected pattern impossible with standard methods. Hence, depending on the detection mode used on the PD station, the mirror is either set in collimating mode for highest angular resolution or at a bending radius value of 10 km in order to ensure a Gaussian shape beam profile with 1 mm FWHM at the sample position.

The final major optical component, located in the experimental hutch, allows focusing the beam on the HP/MD station (at 31 m) and, notably, on the PD station as well (at 35 m), though the latter option has not been commissioned so far by lack of a scientific case. The beam focusing device consists of two independent elliptically bent reflecting surfaces set in KB geometry. On MSPD, the reflecting surfaces are graded $[W/Si]_{110}$ and $[W/Si]_{150}$ multilayers with average layer spacing $d_v = 2.96$ nm and $d_h = 2.57$ nm for vertical and horizontal focusing. The first harmonics of the multilayer reflection is used. Mirrors are positioned 1.1 m and 0.7 m before HP/MD sample position for vertical and horizontal focusing, respectively. Mirror dimensions, bending parameters and multilayer choice have been appropriately selected to operate in the 20 to 50 keV energy range with 75%/90% reflectivity at 20 keV/50 keV and mean energy resolution $\Delta E/E = 2.5\%/1.8\%$ for vertical/horizontal mirror. Indeed, higher energies, hence higher penetration depths, are preferred on angular dispersive HP stations since the monochromatic beam is expected to pass through relatively massive DAC. With this device we got a minimum beam size of pure lorentzian shape with $15 \times 15\,\mu m^2$ FWHM at the HP/MD sample position. Note that the characteristic tails of lorentzian profile lead to an extended effective beam size, typically $45 \times 45\,\mu m^2$ full width at 10% of the maximum intensity, which has to be taken into account when collecting data. In order to minimize the tail contribution —so-called "beam cleaning"— a 50 μm diameter pin hole drilled in a 200 μm thick Pt foil is positioned before the sample. When using the PD station, the KB setup is positioned in such a way that the monochromatic beam can pass between the mirror pair and a 40 mm diameter pipe is quickly mounted between the KB vessel downstream flange and the first component of the PD station. When operating at softer energies (< 10 keV), the pipe and the KB vessel can be evacuated in order to minimize beam absorption.

Finally, beam defining slit systems, intensity monitors and beam imaging devices are positioned at key positions all along the beam. A water-cooled beam defining slit system and a water-cooled beam imaging viewer (CVD foil positioned at 45 deg surveyed by a CCD camera) are located between the mirror and the monochromator. A PIN diode positioned in the monochromator vessel and facing the 1st crystal allows measuring the I_{in} beam intensity impinging the mono. Beam defining slits, a beam imaging viewer (YAG foil positioned at 45 deg surveyed by a CCD camera) and an intensity monitor are located just after the mono. The latter intensity monitor measures I_{out}, which is used, in conjunction with the I_{in} signal, by the 2nd crystal feedback system to maintain the I_{out}/I_{in} ratio at 90% of its maximum value.

3.2 The experimental stations

The techniques used on the High Pressure (HP)/Micro Diffraction (MD) station consist in collecting data in the hard X-ray regime and in transmission geometry from powder samples using a very small beam and a 2-dimensional detector. In the HP case, we can typically study phase transition in materials up to 50 GPa, whereas for MD we can get structural information in different regions of a same sample with high spatial resolution. The HP/MD "diffractometer" essentially consists of two towers of stacked rotation, tilt and translation stages supplied by Huber Diffraktionstechnik (fig. 6, left). The sample is mounted on a tower consisting, from bottom to top, of a XYZ stage, a rotation stage and a XY stage (here Y and Z refers to the direction along and vertical relative to the beam, respectively). This configuration allows aligning a very small sample ($< 50\,\mu$m) on the sample stage rotation axis, and then the rotation axis and sample into the beam. The alignment of the sample on the rotation axis is essential as data are generally collected during rotating the sample over typical 5–30 deg range, which is needed to increase powder averaging. The detector of the HP/MD station is a Rayonix SX165 with 2048×2048 pixels of $80 \times 80\,\mu m^2$ dimension. The detector is mounted on a tower consisting of a X, Y and Z translations, a rotation and a tilt stages. The read-out time of the detector is 3.5 s and typical acquisition time ranges from 5 to 60 s. The sample-detector distance ranges from 100 mm to 500 mm. Actually, high-pressure measurements are performed at room temperature only using hand screw or gas membrane driven DAC. The former are from ALMAX, the latter from BETSA. An *in situ* pressure calibration setup,

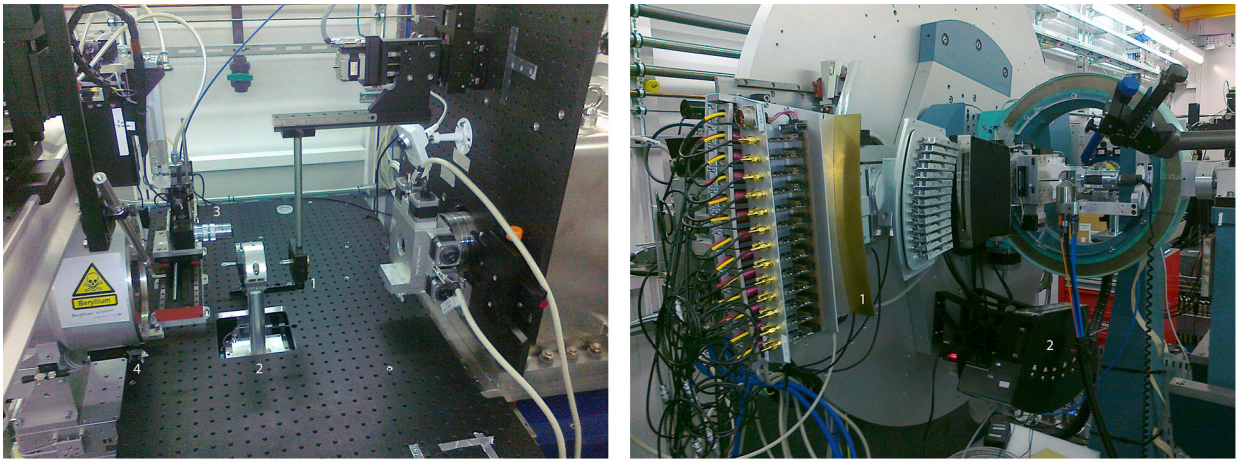

(a) (b)

Fig. 6. (Left) HP/MD station with 1) pinhole support, 2) Diamond anvil Cell (DAC) support, 3) pressure calibration setup 4) 2D detector with beam stop just before. (Right) PD station with 1) MAD detection setup 2) MYTHEN detector. The protection covers of the MAD detection setup have been removed to make individual analyzer/PMT tube channel visible.

based on the ruby fluorescent technique designed and built in house, can be inserted remotely without removing the DAC. For membrane cells, the pressure can be changed remotely as well. The beamline is equipped with a dedicated laboratory for loading DAC using liquid-based pressure transmitting medium. It has appropriate binoculars and an additional pressure calibration setup. In spring 2015, HP measurements will be possible at temperatures up to 300 °C in air. Recently, the demand for micro-diffraction emerged. At MSPD mesh scanning diffraction, and therefore crystalline phase identification, can be performed with good spatial resolution, owing to the small spot size. This technique is widely used in cultural heritage samples, typically in painting or ceramics, in order to reveal the constituents used for specific colors of the samples. Either in HP or in MD techniques, the 2D data are generally processed by radial integration using the Fit2D software [16] which is freely available for various platforms (Linux, Windows). In specific cases, the 2-dimensional feature of the detector is used for analyzing texture and anisotropic strain at selected positions of polycrystalline samples deposited on glass or Si wafer substrates. Owing to the high X-ray energy (> 20 keV) measurements can be done in transmission geometry. For MD data collection, a specific on-axis visualization system has been developed and built at Alba. The beam is passing through a 2 mm hole drilled in an angle of 45 deg *versus* beam positioned mirror that reflects the image of the sample. Appropriate optics inserted between the mirror and a standard CCD camera allow a 12× magnification.

Downstream of the HP/MD station, located 35 m form the source, stands the Powder Diffraction (PD) station (fig. 6, right). Here, powder diffraction patterns are collected in transmission geometry from samples generally enclosed in capillaries. The PD station is essentially a heavy duty 3 concentric circles diffractometer from Huber diffractions technique with two types of detection systems. On the outer circle is mounted the so-called multianalyzer detector (MAD), which is an array of 13-channels crystal analyzer/YAP scintillator/photomultiplier tubes (YAP stands for Ce doped $YAlO_3$ perovskite). The conceptual design of this MAD setup has been extensively described in [17]. Either the (111) or (220) silicon Bragg reflections can be selected for the analyzers. The MAD detector is operational in the whole energy range, 8–50 keV, of the beamline. With this setup, data are collected by scanning the MAD at constant speed, typically 0.5–2 deg/min. The 1.5 deg spacing between detection channels implies that an 18 deg powder pattern, without gap, can in principle be collected within a few minutes. However, a wider scanning range, hence a longer acquisition time, is necessary in order to correctly compensate for unequal efficiencies between channels and to obtain satisfactory statistics, the latter factor, however, being strongly sample-dependent. The data processing software merging the patterns collected by each of the 13 channels is basically the same as the one developed and used on the powder diffraction beamline of the ESRF [18].

Inserting an analyzer, sometimes referred as back monochromator, between the sample and the detector is well known to improve the angular resolution and the signal to noise ratio [19]. Indeed, the limited energy band pass of the analyzer contributes to the elimination of non-elastic scattering processes. Note that the restricted energy band pass allows to use the relatively poor energy resolving YAP scintillator based detectors ($\Delta E/E \sim 10$–60% over 50–7 keV). Since diffracted X-rays are the result of an additional Bragg reflection law with limited angular band pass, the analyzer crystals act as additional tiny aperture slits, hence limiting peak broadening induced by the residual divergence of the beam impinging on the sample, by the size of the sample and by the slight displacement of the sample away from the center of rotation of the diffractometer (*e.g.* wobbling). Finally, the MAD setup on MSPD allows operation with the mirror in collimating mode, achieving the highest possible angular resolution obtainable with the actual MSPD

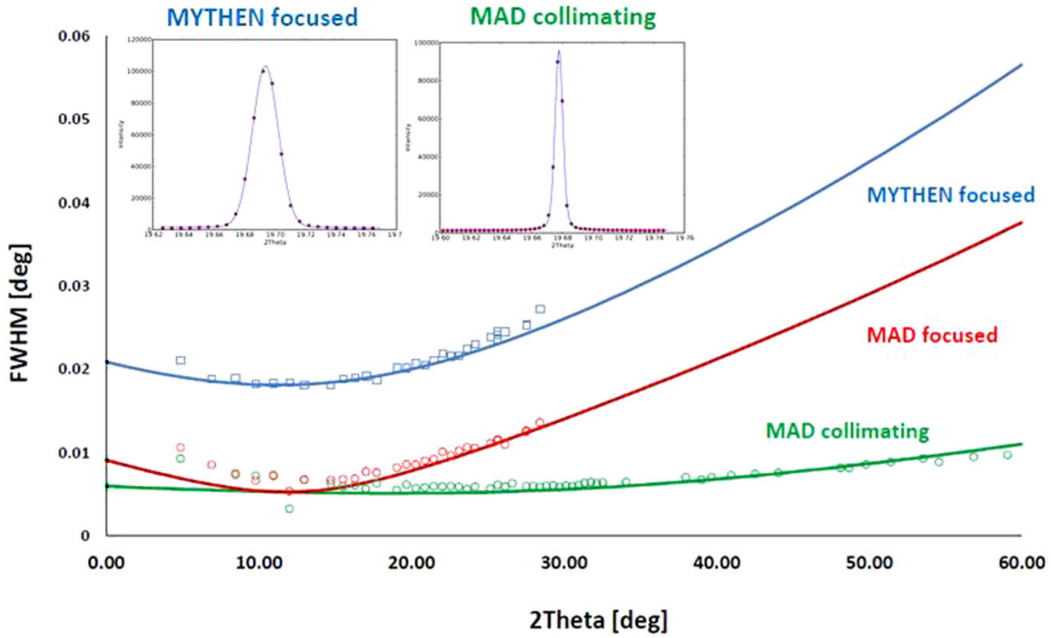

Fig. 7. Instrumental resolution obtained on MSPD at 20 keV using the detector MYTHEN and MAD and with mirror in focusing and/or collimating mode. Points represent individually fitted peaks whereas lines correspond to the resolution obtained from Rietveld refinement. As inset, we have represented the 440 ($2\theta \sim 19.7$ deg) peak of the measured sample, $NaCaAlF_3$, which was enclosed in a 0.5 mm diameter capillary.

instrumental optics component setup. As measured from NaCaAlF2 sample (NAC, fig. 7) which is known to exhibit negligible sample broadening contribution, the minimal achieved peak broadening is 0.004 deg FWHM at 39 keV, which corresponds to a d-spacing resolution $\Delta d/d = 8 \times 10^{-4}$ and $\Delta d/d = 4.4 \times 10^{-4}$ using Si_{111} and Si_{220} reflection of the analyzer, respectively. At high energies (> 30 keV), the Si_{220} reflection of analyzer crystals is preferred because of the higher Bragg angle. This avoids cross-talk between detection channels and, in addition, shifts the minimum angular resolution value towards higher 2θ, where peak overlap is higher. Despite a smaller intrinsic angular band pass, the higher structure factor of the 220 reflection lead to similar reflectivity compared to the 111.

The middle circle is supporting the high-throughput solid-state position-sensitive detector, commercially known as the MYHTEN-II detector [20]. The complete detector is built of 6 single modules of 300 μm thick Si material on which 1280 electrode strips with 50 μm pitch are deposited. The sample to detector distance is 550 mm. This 1-dimensional detection setup allows single shot acquisition of powder patterns in $\sim 40°$ angular range in 0.006 deg steps at ms time resolution and with negligible electronic noise contribution. A typical powder pattern is collected by merging multiple position data with acquisition time ranging from 1 to 60 seconds. Note that a single position data acquisition leads to gaps in the powder pattern at the position between two detection modules. An increase in the number of positions and a decrease in the acquisition time results in a smoother background signal coming from sample holder and air scattering. This is particularly important when the collected data are to be processed by the Pair Distribution Function (PDF) analysis techniques. Here, the most critical signal is expressed as modulations in the background at very high reciprocal space vector values $Q = 4\pi/\lambda \sin(\theta)$, where λ is the X-ray wavelength and 2θ the scattering angle. The X-ray detection principle of solid state position sensitive detectors makes them less efficient with increasing energy. At MSPD, the MYHTEN detection setup is operating satisfactorily up to 30 keV. With a maximum angle of 130 deg, we can hence collect good statistics data up to $Q_{max} = 27$ Å^{-1} reciprocal space values in 10–30 min acquisition time, which is quite competitive for PDF or total scattering data analysis. In such open detection systems, the angular resolution is dominated by the footprint height of the beam on the sample. For samples generally enclosed in glass capillaries, the smaller the diameter, the better the angular resolution. On the other hand, the peak shape is reflecting the vertical profile of the beam impinging on the sample. As explained in the previous paragraph, it is for this reason that we are collecting data with the mirror focusing at the MYTHEN detector distance and a maximal beam height of 1 mm at sample position results in a satisfactory angular resolution. In other words, what we lose in angular resolution by operating with a non-collimating beam is recovered by forcing us to use smaller diameter capillaries. The minimal achieved peak broadening measured on a NAC sample is 0.01–0.02 deg FWHM depending on the energy and the capillary size (0.3 to 1 mm diameter) (fig. 7). Raw data collected by the MYTHEN detector are processed (conversion to angular pattern, merging of multiple positions including proper monitoring of each position, flat field correction, bad channel rejection) either inline and/or offline using an in-house developed Python-based code.

The inner circles support a Huber 512.1-type Eulerian cradle that mounts the samples within a sphere of confusion accuracy of up to 20 μm. In addition to the usual phi and chi axis offered by Eulerian cradles, the sample is further mounted on a XYZ translation stage. Although the cradle can be optionally removed, this operation remains delicate; it has hence been decided to adapt the sample environments to fit within the cradle. Due the limited space between the sample mounting surface and the cradle/diffractometer center of rotation (55 mm), we had to design and build a dedicated, compact "flat" spinner. For mounting samples in the data collection position, we insert the capillaries in brass pins with an inner hole of diameter matching that of the capillary. The brass pin is then mounted/screwed on SPINE like magnetic bases. This allows for straightforward and fast exchange of the samples. A camera coupled to magnifying level optics allows to survey the proper rotation of the capillary (absence of excessive precession) and to precisely align the sample in the beam. The sample can be remotely translated along the rotation axis, which is particularly useful for samples sensitive to radiation damage and/or to collect data at selected positions of the capillary. A XIA brand fast shutter ensures that the samples are illuminated only during effective data integration. Actually, data in temperature ranges of 80–480 K and RT-950 C can be collected using a liquid-nitrogen cryostream and a hot air blower, respectively. A compact liquid helium flow cryostat, which can be mounted in the cradle, has been designed and ordered at the ESRF, Grenoble. The environment will cover a 10–300 K temperature range and will be available in spring 2015.

4 Scientific output

4.1 BL13- XALOC scientific output

Full operation of the BL13-XALOC beamline started fall 2012, already performing MX wavelength-dependent (MAD/SAD) and robot-assisted experiments from the first day. In its short operative life, the beamline has demonstrated the ability to deal with a large variety of data-collection scenarios ranging from standard, routinely automatized, X-ray diffraction experiments to experiments that require more human intervention like dealing with microcrystals or large unit cells. The beamline has exploited to date the anomalous signals from a variety of K (S, Cd, Mn, I, Fe, Ni, Cu, Zn, Se and Br) and L_{III} (Ho, Os, Sm, Gd, Ir, Pt, Au and Hg) absorption edges. From the start of user operation until March 2014, 65 research groups have tested $\sim$ 11000 crystals and collected $\sim$ 4000 datasets (defining one dataset as having 90 or more image frames), which has allowed the users to solve a large variety of macromolecular structures. The beamline has also been instrumental to solve the structure of small organic molecules such as adenine down to a very high resolution (0.45 Å), and highly disordered metallo-organic frameworks [21]. The beamline has been also employed to host cultural heritage experiments, in which the fluorescence and the diffraction signatures were extracted from Gothic paintings, sampled every 6 μm in depth [22].

The structural study of Auxin Response Factors complexed with DNA is a good example of the research carried out at BL13-XALOC beamline. Auxins are plant hormones that control growth and development, that is to say, they determine the size and structure of the plant. Among their many activities, auxins favor cell growth, root initiation, flowering, fruit setting and delay ripening. Auxins have practical applications and are used in agriculture to produce seedless fruit, to prevent fruit drop, and to promote rooting, in addition to being used as herbicides. The biomedical applications of these hormones as anti-tumor agents and to facilitate somatic cell reprogramming (the cells that form tissues) to stem cells are also being investigated.

The effects of auxins in plants were first observed by Darwin in 1881, and since then this hormone has been the focus of many studies. However, although it was known how and where auxin is synthesized in the plant, how it is transported, and on which receptors it acts, it was unclear how a hormone can trigger such diverse responses.

At the molecular level, the hormone serves to unblock a transcription factor, a DNA-binding protein, which in turn activates or represses a specific group of genes. Some plants have more than 20 of such auxin-regulated transcription factors, which are called ARFs (Auxin Response Factors). They control the expression of numerous plant genes in function of the task to be undertaken, that is to say, cell growth, flowering, root initiation, leaf growth, etc.

The structural basis of the regulation of auxin-dependent gene expression has been elucidated by macromolecular crystallography using the XALOC beamline and some beamlines at the ESRF (Grenoble, France) [23]. The atomic structure of ARFs bound to regions of DNA that control gene expression has revealed that the DNA-binding domain (DBD) of ARFs recognize DNA as dimers (fig. 8). This study also shows that the local recognition of DNA is highly similar for gene production activator or repressor ARFs, that is, the recognition of DNA by an ARF (DBD) dimer is independent of the functionality of the ARF. This indicates that functional differences must be related to the formation of higher order structures that most probably involve distant regions within the genomic DNA.

4.2 BL04-MSPD scientific output

The high-pressure station opened to friendly and official users' experiments starting June 2012 and has already produced numerous peer-reviewed publications [24–29]. Most of them deal with crystal structure studies of inorganic materials and/or crystal structure transition as a function of the pressure, or equation of state determination. HP X-ray diffraction experiments are generally complementary of Raman spectroscopy data and/or density functional theory calculations.

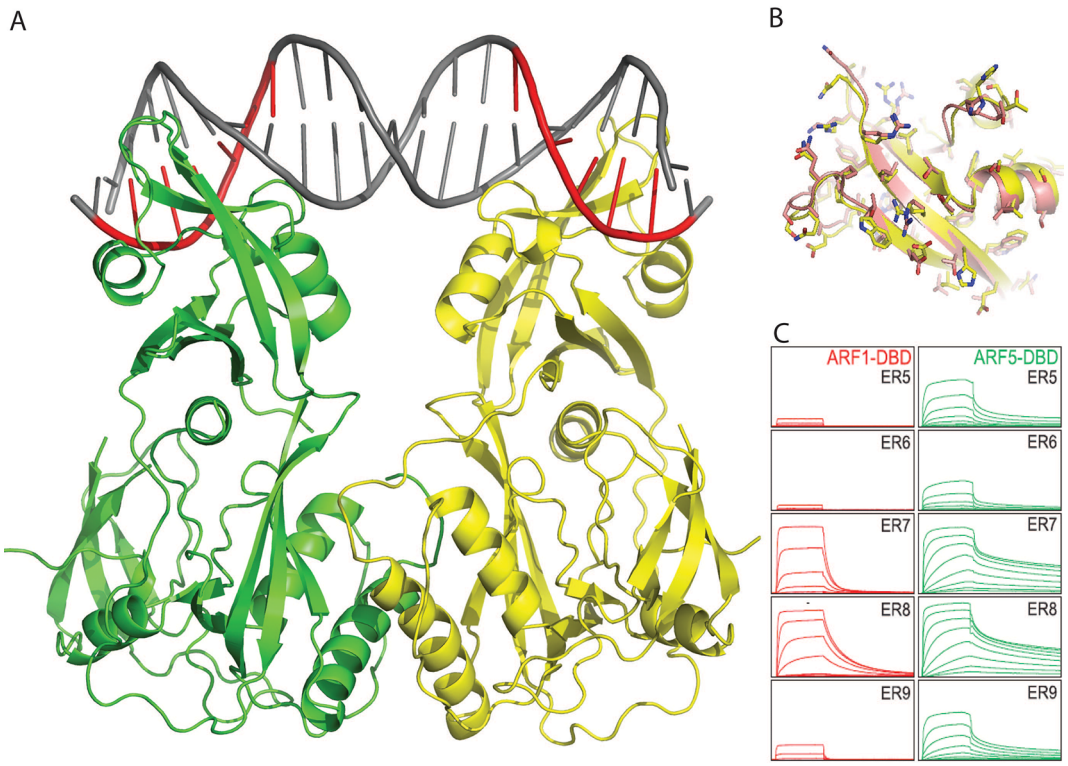

Fig. 8. The DNA-binding domains of ARF1 (shown in yellow and green) dimerize and in this way recognize the two binding sites on a DNA fragment (A). The residues that recognize the DNA are highly conserved among many of the ARFs. Panel B shows these residues for ARF1 and ARF5, However, the two different ARFs distinguish between DNA fragments based on the distance between the two sites (C), that is, on the length of the spacer.

The powder diffraction station opened to users in October 2012 and February 2013 for measurements with the MYTHEN and MAD detection system, respectively. The high angular resolution setup has proven useful for determining the effective crystal structure of the positive electrode material $Na_3V_2(PO_4)F_3$ which, in contrast to previous numerous studies predicting a tetragonal structure at room temperature appears to be orthorhombic but with a phase transition to a tetragonal phase at 400 K [30]. The crystal structure of the new zeolite system, named as ITQ52, could be resolved using *ab initio* techniques within the space group I2/m, with cell parameters $a = 17.511$ Å, $b = 17.907$ Å, $c = 12.367$ Å, and $\beta = 90.22$ deg [31]. Here, the high angular data collected on MSPD appeared essential to unambiguously determine the structure.

Owing to its fast acquisition speed, the MYTHEN based detection setup was essentially used in structure characterization of systems under the influence of external parameters, the most typical one being temperature, or during the kinetics of chemical processes. This is nicely illustrated in the study of cement-based materials at MSPD, during which the transformation of the starting phases in the material is tracked during hydration [32,33]. Another applied physics example concerns the study of battery-based materials for which the electrochemical process can be studied in operando during the charging and discharging process [34]. In addition, the high intensity mode offered by the MYTHEN allows for short acquisition times, which allows the observation of minority phases —down to 1% amount— within a majority crystalline phase matrix. The feature is of interest in the pharmaceutical applications aimed at identifying and quantifying the crystalline form of active pharmaceutical ingredients.

5 Conclusions

The Alba synchrotron radiation facility, built close to Barcelona (Spain), entered into user operation in 2012 with two insertion device beamlines, out of seven, fully dedicated to crystallography techniques. Alba is currently running in top-up mode, and has offered about 4500 h of beam in the year 2014.

The BL13-XALOC beamline is dedicated to macromolecular crystallography and is equipped with state-of-the-art instrumentation including a high-accuracy diffractometer with a removable mini-kappa mount, an automated mounting robot and a photon-counting 6-Mpixel detector. The beam delivered at the sample position can be easily tuned between 5.5 and 22 keV and is focused to a spot size of $52 \times 5.5\,\mu m^2$ beam FWHM (H × V), with a flux of $\sim 2 \times 10^{12}$ photons s^{-1} with a current of 250 mA in the storage ring. The beam can be readily defocused to produce a beam size of $200 \times 200\,\mu m^2$ without loss of flux or significant beam profile striations.

With its high angular resolution setup, the PD station of the material science powder diffraction beamline (BL04-MSPD) is at the top level of powder diffraction beamlines in the world. The high-throughput MYTHEN detector certainly represents an added value since it allows fast kinetics and/or operando measurements. Based on the number of already published, among them the first arising from Alba data collection, the HP station has already proven its high standard level.

Both beamlines are currently under routine user operation, delivering continuous, high-impact scientific output on a large variety of crystallography-related fields. Access to academic beamtime is open to worldwide scientific community through the Alba user portal (`http://useroffice.cells.es`). Beamtime is also accessible via commercial/industrial basis.

References

1. D. Einfeld, in *Proceedings of the Second International Particle Accelerator (IPAC 2011)*, San Sebastián, 2011.
2. J. Campmany, J. Marcos, V. Massana, F. Becheri, J.V. Gigante, J. Phys. Conf. Ser. **425**, 032010 (2013).
3. Jordi Juanhuix, Fernando Gil-Ortiz, Guifré Cuní, Carles Colldelram, Josep Nicolás, Julio Lidón, Eva Boter, Claude Ruget, Salvador Ferrer, Jordi Benach, J. Synchrotron Radiat. **21**, 679 (2014).
4. P. Kirkpatrick, A.V. Baez, J. Opt. Soc. Am. **38**, 766 (1948).
5. T. Moreno, R. Belkhou, G. Cauchon, M. Idir, Proc. SPIE **5921**, 59210F (2005).
6. J. Nicolás, C. Ruget, J. Juanhuix, J. Benach, S. Ferrer, J. Phys. Conf. Ser. **425**, 052016 (2013).
7. J. Nicolás, J.C. Martínez, Nucl. Instrum. Methods Phys. Res. A **710**, 24 (2013).
8. J. Ohana, L. Jacquamet, J. Joly, A. Bertoni, P. Taunier, L. Michel, P. Charrault, M. Pirocchi, P. Carpentier, F. Borel, R. Kahn, J.-L. Ferrer, J. Appl. Cryst. **37**, 72 (2004).
9. C. Broennimann, E.F. Eikenberry, R. Horisberger, G. Hülsen, B. Schmitt, C. Schulze-Briese, T. Tomizaki, Nucl. Instrum. Methods Phys. Res. A **510**, 24 (2003).
10. T. Coutinho, G. Cuní, D. Fernández-Carreiras, J. Klora, C. Pascual-Izarra, Z. Reszela, R. Suñé, in *Proceedings of the 13th International Conference on Accelerator and Large Experimental Physics Control Systems (ICALEPCS2011)*, Grenoble, France, 2011.
11. F. Fauth, I. Peral, C. Popescu, M. Knapp, Powder Diffr. **28**, S360 (2013).
12. M. Knapp, I. Peral, L. Nikitina, M. Quispe, S. Ferrer, Z. Kristallogr. Proc. **1**, 137 (2011).
13. T. Tanaka, H. Kitamura, J. Synchrotron Radiat. **8**, 1221 (2001).
14. F. Gozzo, B. Schmitt, Th. Bortolamedi, C. Giannini, A. Guagliardi, M. Lange, J. Alloys Compd. **362**, 206 (2004).
15. Josep Nicolas, Gastón García, Proc. SPIE **8848**, 884810 (2013).
16. A.P. Hammersley, S.O. Svensson, M. Hanfland, A.N. Fitch, D. Häusermann, High Pressure Res. **14**, 235 (1996).
17. I. Peral, J. McKinlay, M. Knapp, S. Ferrer, J. Synchrotron Radiat. **18**, 1 (2011).
18. Jon P. Wright, Gavin B.M. Vaughan, Andy N. Fitch, *Merging Data From a Multi-Detector Continuous Scanning Powder Diffraction System* (International Union of Crystallography, Computing Commission, 2003).
19. D.E. Cox, J.B. Hastings, W. Thomlinson, C.T. Prewitt, Nucl. Instrum. Methods Phys. Res. **208**, 573 (1983).
20. Anna Bergamaschi, Antonio Cervellino, Roberto Dinapoli, Fabia Gozzo, J. Synchrotron Radiat. **17**, 653 (2010).
21. Cristina García-Simón, Marc Garcia-Borràs, Laura Gómez, Teodor Parella, Sílvia Osuna, Jordi Juanhuix, Inhar Imaz, Daniel Maspoch, Miquel Costas, Xavi Ribas, Nature Commun. **5**, 5557 (2014).
22. Nati Salvadó, salvador Butí, Gianfelice Cinque, Jordi Juanhuix, Carme Clemente, Victòria Beltran, Trinitat Pradell, *Synchrotron Radiation based techniques for the study of altered metal foil coatings in Baroque altarpieces*, in *Synchrotron Radiation and Neutrons in Art and Archaeology (SR2A-2014)* (Musée du Louvre, Paris, 2014).
23. Roeland Boer, Alejandra Freire-Rios, Willy A.M. van den Berg, Terrens Saaki, Iain W. Manfield, Stefan Kepinski, Irene López-Vidrieo, Jose Manuel Franco-Zorrilla, Sacco C. de Vries, Roberto Solano, Dolf Weijers, Miquel Coll, Cell **156**, 577 (2014).
24. J.A. Barreda-Argueso, S. Lopez-Moreno, M.N. Sanz-Ortiz, F. Aguado, R. Valiente, J. Gonzalez, F. Rodrıguez,1 A.H. Romero, A. Munoz, L. Nataf, F. Baudelet, Phys. Rev. B **88**, 2014108 (2013).
25. Daniel Errandonea, Oscar Gomis, Braulio García-Domene, Julio Pellicer-Porres, Vasundhara Katari, S. Nagabhusan Achary, Avesh K. Tyagi, Catalin Popescu, Inorg. Chem. **52**, 12790 (2013).
26. A.L.J. Pereira, D. Errandonea, A. Beltran, L. Gracia, O. Gomis, J.A. Sans, B. Garcia-Domene, A. Miquel-Veyrat, F.J. Manjon, A. Munoz, C. Popescu, J. Phys.: Condens. Matter **25**, 475402 (2013).
27. David Santamaría-Pérez, Enrico Bandiello, Daniel Errandonea, Javier Ruiz-Fuertes, Oscar Gomis, Juan Angel Sans, Francisco Javier Manjón, Plácida Rodríguez-Hernández, Alfonso Muñoz, J. Phys. Chem. C **117**, 12239 (2013).
28. D. Errandonea, C. Popescu, S.N. Achary, A.K. Tyagi, M. Bettinelli, Mater. Res. Bull. **50**, 279 (2014).
29. Alka B. Garg, D. Errandonea, P. Rodríguez-Hernández, S. López-Moreno, A. Muñoz, C. Popescu, J. Phys.: Condens. Matter **26**, 265402 (2014).
30. M. Bianchini, N. Brisset, F. Fauth, F. Weill, E. Elkaim, E. Suard, C. Masquelier, L. Croguennec, Chem. Mater. **26**, 4238 (2014).
31. Raquel Simancas, Jose L. Jordaì, Fernando Rey, Avelino Corma, Angel Cantín, Inma Peral, C. Popescu, J. Am. Chem. Soc. **136**, 3342 (2014).

32. G. Álvarez-Pinazo, A. Cuesta, M. García-Maté, I. Santacruz, E.R. Losilla, S.G. Sanfélix, F. Fauth, M.A.G. Aranda, A.G. De la Torre, Cem. Concr. Res. **56**, 12 (2014).
33. A. Cuesta, G. Álvarez-Pinazo, S.G. Sanfélix, I. Peral, M.A.G. Aranda, A.G. De la Torre, Cem. Concr. Res. **63**, 127 (2014).
34. Murat Yavuz, Nilüfer Kiziltas-Yavuz, Aiswarya Bhaskar, Marco Scheuermann, Sylvio Indris, Francois Fauth, Michael Knapp, Helmut Ehrenberg, Z. Anorg. Allg. Chem. **640**, 3118 (2014).